

MAGNETIZED GRB REVERSE SHOCK: DENSITY-FLUCTUATION-INDUCED FIELD DISTORTION AND POLARIZATION DEGREE REDUCTION IN EARLY AFTERGLOWS

WEI DENG (邓巍)^{1,2}, BING ZHANG (张冰)¹, HUI LI (李晖)², JAMES M. STONE³¹Department of Physics and Astronomy, University of Nevada Las Vegas, Las Vegas, NV 89154, USA; deng@physics.unlv.edu, zhang@physics.unlv.edu²Los Alamos National Laboratory, Los Alamos, NM 87545, USA; hli@lanl.gov and³Department of Astrophysical Sciences, Princeton University, Princeton, NJ 08544-1001, USA; jstone@astro.princeton.edu

ABSTRACT

The early optical afterglow emission of several gamma-ray bursts (GRBs) shows a high linear polarization degree (PD) of tens of percent, suggesting an ordered magnetic field in the emission region. The lightcurves are consistent with being of a reverse shock (RS) origin. However, the magnetization parameter, σ , of the outflow is unknown. If σ is too small, an ordered field in the RS may be quickly randomized due to turbulence driven by various perturbations so that the PD may not be as high as observed. Here we use the “Athena++” relativistic MHD code to simulate a GRB jet with ordered magnetic field propagating into a clumpy ambient medium, with a focus on how density fluctuations may distort the ordered magnetic field and reduce PD in the RS emission for different σ values. For a given density fluctuation, we discover a clear power law relationship between the relative PD reduction and the σ value of the outflow. Such a relation may be applied to estimate σ of the GRB outflows using the polarization data of early afterglows.

Subject headings: gamma-ray burst: general - galaxies: jets - polarization - magnetic fields - shock waves - magnetohydrodynamics (MHD)

1. INTRODUCTION

The jet composition and energy dissipation, particle acceleration and radiation mechanisms of GRBs are not identified and subject to debate (Kumar & Zhang 2015, for a recent review). Leading models include matter-dominated fireball shock model (e.g. Paczynski 1986; Goodman 1986; Rees & Meszaros 1994; Mészáros & Rees 2000) and Poynting-flux-dominated magnetic dissipation models (e.g. Lyutikov & Blandford 2003; Zhang & Yan 2011; McKinney & Uzdensky 2012; Deng et al. 2015, 2016). Growing evidence suggests that the GRB jets carry a dynamically important magnetic field, so that magnetic reconnection may play an important role in producing observed GRB prompt emission and afterglow emission.

One piece of such evidence comes from the observations of the early optical afterglow of GRBs, which is dominated by a rapidly decaying ($\propto t^{-2}$) segment early on from the external reverse shock (RS) (Akerlof et al. 1999; Sari & Piran 1999; Mészáros & Rees 1999; Gomboc et al. 2008; Gao et al. 2015). Modeling such a component suggests that the RS is more magnetized than the forward shock (FS), so that the GRB jet is more magnetized than the ambient medium (Fan et al. 2002; Zhang et al. 2003; Kumar & Panaitescu 2003; Zhang & Kobayashi 2005). This is consistent with the scenario that prompt emission is powered by magnetic reconnection and turbulence with a moderate magnetization parameter σ in the prompt emission region (Zhang & Yan 2011), while when the jet is decelerated by an ambient medium (when the RS propagates through the ejecta), the σ value of the ejecta cannot be very high (otherwise the RS is weak or suppressed, Zhang & Kobayashi 2005; Mimica et al. 2009; Mizuno et al. 2009).

A direct proof of such a scenario comes from the polarization observations of early optical emission of some

GRBs. Steele et al. (2009) discovered a $\sim 10\%$ polarization degree (PD) of the early RS optical emission from GRB 090102. Mundell et al. (2013) for the first time measured the “polarization lightcurve” of GRB 120308A, which shows a $\sim 28\%$ PD at 4 minutes after the GRB, which is reduced to $\sim 16\%$ PD over the subsequent 10 minutes as the FS emission contribution becomes stronger. These observations suggest that there exists an ordered magnetic field in the RS region (Lan et al. 2016). However, the σ value of the RS emission cannot be easily diagnosed based on the PD and lightcurve data.

For a relativistic outflow, strong turbulence is likely developed in the flow due to various perturbation mechanisms (e.g. density clumps in the ambient medium or intrinsic irregularity within the flow). If $\sigma \ll 1$, even if an ordered magnetic field configuration may exist initially, turbulence may quickly randomize the field configurations, which would greatly reduce the ordered field component and the resulting PD from synchrotron radiation. As a result, based on the observed PDs of GRBs 090102 and 120308A, one may be able to place a lower limit of the σ values of the outflows. To do this, detailed numerical simulations are needed.

In this paper, we report our first effort to simulate the distortion of magnetic fields in RS region of a relativistic jet due to density fluctuations, as well as the resultant reduction of the PD of synchrotron radiation.

2. PROBLEM SETUP

We use the relativistic MHD code “Athena++” (White et al. 2016) to simulate the dynamical evolution of the outflow, and the “3DPol” multi-zone polarization-dependent ray-tracing radiation code (Zhang et al. 2014) to model the PD of synchrotron radiation in the RS region.

We apply a planar shock geometry to simplify the prob-

lem in this investigation. This is relevant if the jet is “cylindrical”. In principle, a GRB jet may be “conical”, so that additional effects, such as the Rayleigh-Taylor (RT) instability (Duffell & MacFadyen 2013) may operate, which would further distort the ordered magnetic fields and reduce the PD. To drive turbulence in the RS region, we introduce a density fluctuation in the ambient medium. In principle, the ordered magnetic fields after prompt emission should be already distorted so that a certain random component coexists with the ordered component. However, to simplify the problem, we assume a completely ordered B field in the jet with uniform strength and direction. For a relativistic emitter, and observer would only observe a solid angle with half opening angle of $\sim 1/\Gamma$ (Γ is Lorentz factor). The observed PD would be somewhat reduced within the $1/\Gamma$ cone due to the relativistic Doppler effect (Lazzati 2006). For simplicity we ignore this effect as well. Putting all these simplifications together, the PD results obtained in this paper may be regarded as a conservative upper limit.

We perform our simulation within the “lab” frame, in which the jet propagates with a relativistic speed into an ambient medium at rest. Since the global structure of the jet does not matter much for an observer (who only sees a small patchy of jet within the $1/\Gamma$ cone), we introduce a uniform magnetic field perpendicular to the direction of motion. For the planar geometry, it is convenient to simulate the jet propagation problem using a 2D rather than a 3D box¹. We define that the jet propagates in the z direction, and the lab-frame magnetic field is in the y direction. The effective resolution of the simulations is $\Delta y \approx \Delta z \approx 0.0012L_0$, where L_0 is computational length unit. The entire simulation frames has $20L_0$ in the z direction and $0.156L_0$ in the y direction. A periodic boundary condition is adopted.

The initial setup of the number density distribution is shown in Fig. 1a. The high density ejecta ($n = 100$) and the low density ambient ($n = 1$) are separated at the position $z = 1$. Some density clumps are introduced in the ambient medium to mimic density fluctuation. The density profile of each clump is exponential with the maximum number density equals to 100 in the center. The initial magnetic field is set to have B_y only (Fig. 1c)². Different values of B_y are explored, which correspond to different initial values of the magnetization factor σ in the ejecta. Since the initial thermal energy is much smaller than the kinetic energy, σ can be calculated as $\sigma \approx B^2/4\pi\Gamma^2nm_p c^2$, where m_p is the proton mass and c is the speed of light. The typical Lorentz factor (Γ) of GRBs at the deceleration phase is around several hundred (e.g. Liang et al. 2010), which is too extreme for stable simulations in some parameter space. Hence, we set up two groups with different Γ (10 and 20)³ of the ejecta (Fig. 1b). Although these are smaller than that of

typical GRBs at the deceleration phase, the simulation can nonetheless catch the key physics explored in this paper, and the difference in the results between these two groups can reveal the possible effect of different initial Γ .

The parameters for all the simulation models are listed in Table 1. Model 0 is the reference model without density fluctuation and magnetic field in the jet, which is used to test the basic evolution process of the blast-wave. The simulation results are fully consistent with analytical solutions, suggesting the validity of relativistic Athena++. Models 1-5 have the same density fluctuations but different σ (and hence B_y) in the ejecta. This allows us to explore how magnetic field distortion and the resulting PD vary with σ . Models 6-10 have a different initial Lorentz factor ($\Gamma=20$) corresponding to Models 1-5 ($\Gamma=10$), which is a preliminary test of the effect of Γ . As the jet runs into the medium, four regions are developed: 1. un-shocked medium; 2. shocked medium; 3. shocked jet; 4. un-shocked jet. Our initial conditions define the parameters in regions 1 and 4. In Table 1, the subscripts “4” and “1” denote the un-shocked jet and un-shocked medium, respectively, Γ is the Lorentz factor, n is the number density, and P is the thermal pressure. The parameters are all in the code units, and we can convert them to the physical units if we define a typical length L_0 and a typical magnetic field strength B_0 between the two unit systems (see Table 1 in Deng et al. 2015).

The σ values are set to be below unity based on two considerations: 1. Significant magnetic dissipation likely has occurred during the prompt emission phase (Zhang & Yan 2011; Deng et al. 2015), so that the σ of the outflow has significantly reduced beyond the prompt emission radius. There is a continuous decrease of σ as the jet expands and at the deceleration radius, σ is likely below unity (e.g. Gao & Zhang 2015); 2. The RS is weak or does not exist if σ is above unity (Zhang & Kobayashi 2005; Mimica et al. 2009; Mizuno et al. 2009). Since observationally one does observe the RS emission, σ cannot be too high.

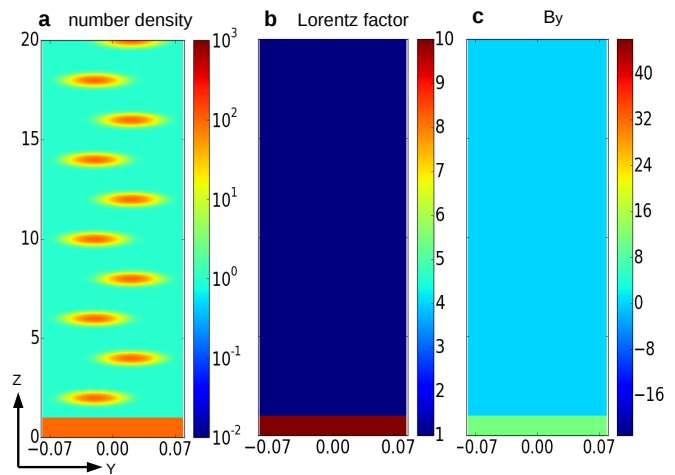


FIG. 1.— The initial setup of the number density distribution (a), the Lorentz factor distribution (b), and the initial magnetic field B_y distribution (c) for Model 3. The front of the jet is located at $z = 1$ initially and propagates upwards to the ambient medium.

¹ Even though the simulation box is essentially 2D, all the vectors are solved in 3D.

² In the co-moving frame, the ejecta carries a uniform B'_y . In the lab frame, one sees a Poynting-flux, with an electric field component in the x direction (E_x) with a similar amplitude as B_y . By setting B_y and Γ in the lab frame, the E_x component is self-consistently incorporated.

³ The upper limit of Γ that code can handle is higher and varies depending on the values of other parameters, e.g. σ .

TABLE 1
THE INITIAL PARAMETERS OF THE SIMULATION MODELS

Group 1: $\Gamma_4 = 10$							
Models	σ_4	$B_{y,4}$	Γ_4	n_4	n_1	P_4	P_1
0	0	0	10	100	1	1	0.01
1	0.1	31.62	10	100	1	1	0.01
2	10^{-2}	10	10	100	1	1	0.01
3	10^{-3}	3.162	10	100	1	1	0.01
4	10^{-4}	1	10	100	1	1	0.01
5	10^{-5}	0.3162	10	100	1	1	0.01
Group 2: $\Gamma_4 = 20$							
Models	σ_4	$B_{y,4}$	Γ_4	n_4	n_1	P_4	P_1
6	0.1	63.24	20	100	1	1	0.01
7	10^{-2}	20	20	100	1	1	0.01
8	10^{-3}	6.324	20	100	1	1	0.01
9	10^{-4}	2	20	100	1	1	0.01
10	10^{-5}	0.6324	20	100	1	1	0.01

3. RESULTS

3.1. The representative case: Model 3

We first present the detailed evolution of a representative case Model 3 ($\sigma = 10^{-3}$). The zoom-in contour plots of the number density (Fig. 2b) and the two components of the magnetic field, B_y (Fig. 2c) and B_z (Fig. 2d) are presented at $t = 8t_0$, where $t_0 = L_0/c$ is the time normalization factor between the code and physical units. As a comparison, we also show the density contour of Model 0 in Fig. 2a. One can see that the surface of the contact discontinuity (CD, the separation between the yellow and the red regions) is highly distorted in Model 3 due to perturbation of the density clumps. Also in the RS region the initially pure ordered magnetic field B_y is distorted significantly and a significant B_z component is generated. This significant topological change of the magnetic field would inevitably lead to the reduction of the synchrotron radiation PD in the RS emission.

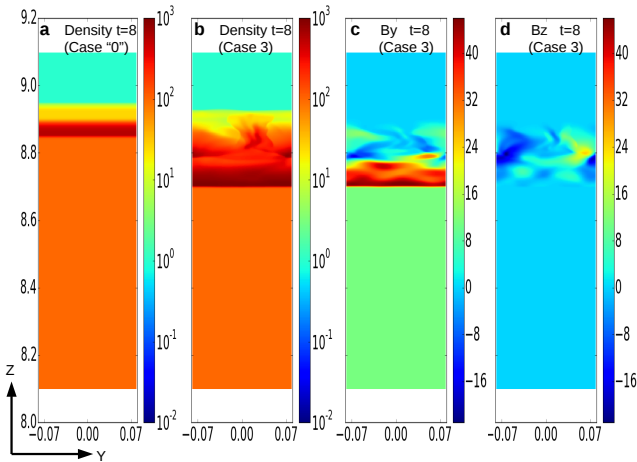


FIG. 2.— Zoom-in cuts of our simulation results for Model 3 ($\sigma = 10^{-3}$) at $t=8t_0$. Panel (a) is the density contour plot of Model 0 as a reference. Panels (b), (c), and (d) are the number density, B_y , and B_z contour plots of Model 3. The magnetic field lines are significantly distorted by the density fluctuations, with a significant B_z component is developed.

Figure 3 shows the synchrotron radiation PD evolution of Model 3. To calculate the polarization evolution, we use the same method used in our previous work (Zhang et

al. 2016; Deng et al. 2016). We first define the region between the CD and the RS in the surface density contour as the region where RS emission comes from. In order to handle the highly distorted CD surface, we develop a numerical approach to define the complex CD profile based on a sharp density discontinuity in the numerical cells. We then uniformly inject particles with a power law energy distribution ($n = n_0(\gamma_e/\gamma_0)^{-2.5}$) in the RS region. Next, we use the “3DPol” multi-zone polarization-dependent ray-tracing radiation code (Zhang et al. 2014) to calculate the evolution of the PD from the RS region based on our MHD simulation results. From Fig. 3, we show that the PD quickly (in $\sim 2t_0$) drops from the initial high value to a lower value. This is caused by the distortion of magnetic fields due to density fluctuations. In long term, the PD gradually recovers due to the resilience of the magnetic field lines. However, we believe that such a recovering effect may be artificial. By considering a more realistic global magnetic configuration (Deng et al. 2015) and the Rayleigh-Taylor instability in the conical shell (Duffell & MacFadyen 2013), one would expect that the distorted B configuration may not be easily recovered. In the following discussion, we focus on the minimum value in the PD curve and use it to define the reduction of PD from the original value.

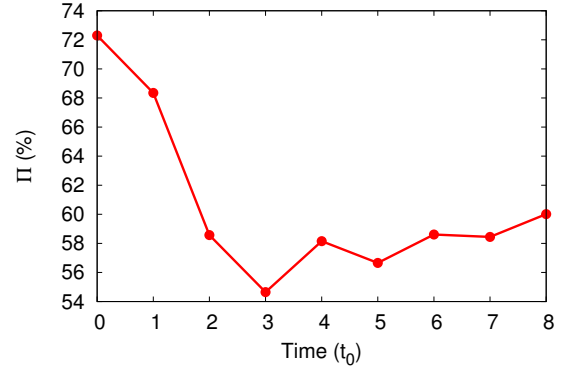


FIG. 3.— The polarization evolution of Model 3 ($\sigma = 10^{-3}$). It shows a significant PD drop initially due to the distortion of the magnetic field by the ambient medium density fluctuation. The later PD gradually increases, but it is mainly due to the simplification of our model and most likely does not exist in the real situations.

3.2. Relationship between PD reduction and σ

We run other Models with different initial σ for each group of Γ_4 , and display the initial PD and final PD in Fig. 4a. For the uniform magnetic field distribution and a planar geometry, the maximum PD allowed for synchrotron radiation, i.e. $\Pi = (p+1)/(p+7/3) \simeq 72\%$ for $p = 2.5$ (Rybicki & Lightman 1979), can be achieved. One can see after density perturbation, the minimum PD in the RS region clearly scales with σ for each group of Γ_4 . The smaller the σ value, the lower the minimum PD. In reality, the field configuration after the prompt emission phase must have been distorted due to magnetic dissipation processes such as internal-collision-induced magnetic reconnection and turbulence (Zhang & Yan 2011; Deng et al. 2015), the initial Π in the RS

crossing phase must be lower than 72%. As a result, the relative PD reduction, defined as $\xi = (\Pi_0 - \Pi_{\min})/\Pi_0$, may be more relevant. This is plotted in Fig. 4b, which clearly shows a decrease of the relative reduction with increasing σ for each group of Γ_4 . Fits to this power law regime ($\sigma = 0.1$ removed) give empirical relations $\xi = 6.0\sigma^{-0.21}$ for the group of $\Gamma_4 = 10$, and $\xi = 1.0\sigma^{-0.37}$ for the group of $\Gamma_4 = 20$.

The behavior may be understood in terms of pressure and energy. One may consider the problem in the rest-frame of the RS region, in which the RS region is a target with growing thickness (as the RS front propagates into the jet) while the density clumps are bullets penetrating into the target. In our simulations, the ram pressure (P_r) and kinetic energy (\mathcal{E}_K) of the density clumps remain the same for different models. The co-moving magnetic pressure ($P_B = B'^2/8\pi$) varies with σ in different models, and the co-moving magnetic energy (\mathcal{E}_B) varies with σ and also with time as the volume of the RS region expands. In all our models, P_r is designated to be greater than P_B , so that the magnetic field configuration can be distorted. When σ is small, the magnetic field is dynamically unimportant. The magnetic amplification factor across the RS front depends on Γ only when the initial density and pressure ratio are fixed, so that the magnetic pressure in the RS region would scale linearly with σ in logarithmic space for each group of Γ_4 . This is indeed seen from the numerical data in Fig. 4c. Since the magnetic pressure is the main stabilizer of the magnetic configuration against density fluctuation perturbation, and the relative PD reduction therefore follows a power-law relation with σ in the $\sigma \ll 1$ regime. We also find that the power-law indices are different between two groups with the different initial Lorentz factor, which means that the indices may be a function of the initial Lorentz factor, the initial density and pressure ratio, and the amplitude of the ambient density perturbation, which need additional investigation in the future.

When σ is higher than 0.01, the magnetic field starts to affect the RS dynamics, which would decrease the RS strength and the compression ratio and in the meantime increase the reverse shock speed in the CD frame. Although the magnetic pressure increases more slowly (Fig. 4b) due to the weaker RS, the thickness of the RS region and hence the magnetic energy increase more rapidly due to the faster RS speed (Zhang & Kobayashi 2005; Mimica et al. 2009; Mizuno et al. 2009). Even though the field configuration close to CD is distorted more, the field configuration from the far end of CD (close to the RS front) is less perturbed due to the larger volume of the RS region so that on average the field configuration in the entire RS region is less perturbed. This explains the roll-over in the $P_B - \sigma$ relation in Fig. 4c, and the relatively small PD reduction at higher σ in Fig. 4b.

4. CONCLUSIONS AND DISCUSSION

In this paper, we explore how resilient a magnetic field is in a relativistic jet against density perturbation from the ambient medium in view of the recent observations of moderately high linear PD in some GRB early optical afterglows (Steele et al. 2009; Mundell et al. 2013). The motivation is to set a possible lower limit on the σ value of the outflow based on the data. In view of the com-

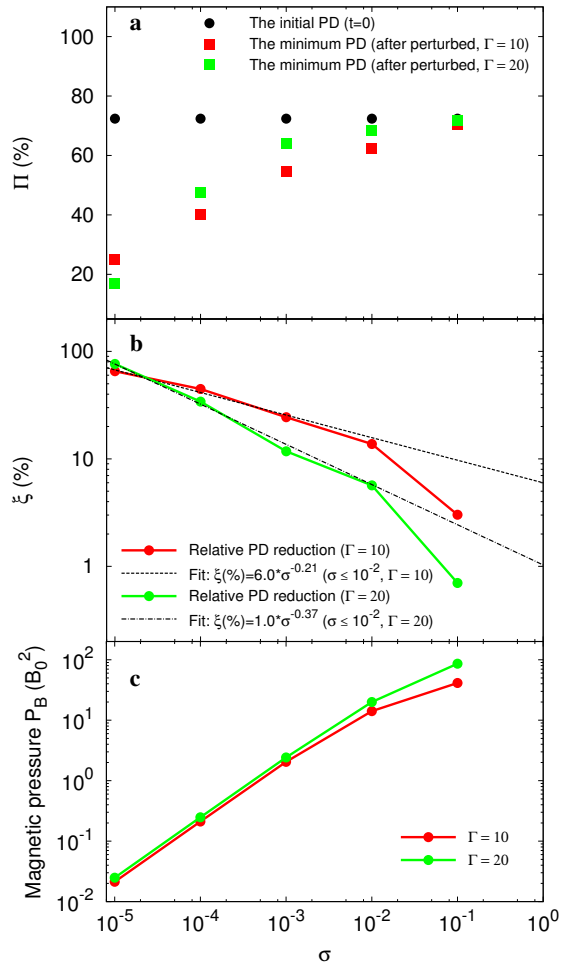


FIG. 4.— (a) The initial and the minimum values of PD during the PD evolution for different initial σ , (b) the relationship between the relative PD reduction and initial σ , and (c) the relationship between the magnetic pressure in the co-moving frame of the RS and σ . Both show a power law relationship when σ is relatively small ($\sigma < 0.01$).

plication of the GRB RS problem, we limit ourselves to a cylindrical jet with a planar geometry with an initial uniform ordered magnetic field configuration. By introducing a perturbation due to density fluctuations from the ambient medium, we investigate how the distortion of magnetic configuration and reduction of PD depend on the σ parameter of the jet. As expected, our numerical simulations using the relativistic Athena++ code show more significant reduction of PD with decreasing σ . The numerical results show an interesting power-law behavior between the relative PD reduction and σ , which may be applied to place constraints on the jet composition of GRBs. For example, if at the end of GRB prompt emission the PD is of $\sim (10\% - 40\%)$ (e.g. Deng et al. 2016), the detection of $\sim 10\%$ PD in GRB 090102 (Steele et al. 2009) and $\sim 28\%$ and 16% in GRB 120308A (Mundell et al. 2013) suggest that the PD is not reduced significantly in the RS region. Since turbulence is ubiquitous in a GRB environment (Zhang & Yan 2011), the preservation of such a moderately high degree of PD suggests a relatively strong B field in the RS region. The low- σ cases (e.g. $\sigma < 10^{-3}$) may be ruled out. This conclu-

sion is consistent with lightcurve modeling of GRB early afterglows that shows a relatively large magnetic microphysics parameter ratios between FS and RS (Fan et al. 2002; Zhang et al. 2003; Kumar & Panaitescu 2003; Gao et al. 2015).

Other effects not included in the current simulations include the possible RT instability in a conical jet geometry, the initial more complicated magnetic configuration directly adopted from our previous simulations of prompt emission (Deng et al. 2015), and the 3D effect which in principle can lead to more tangled fields. We plan to investigate these effects in future more detailed studies. In any case, all these parameters tend to further destroy the ordered magnetic field configurations and reduce the PD in the RS emission. The PD values obtained in this paper are conservative upper limits. The σ constraints using the results obtained from this paper can

be regarded as conservative lower limits.

This work is supported by NASA through grants NNX15AK85G and NNX14AF85G, and by the LANL/LDRD program and Institutional Computing Programs at LANL and by DOE/Office of Fusion Energy Science through CMSO. We thank the important technical support from Christopher White, Xuening Bai, Gustavo Rocha da Silva, Zhaohuan Zhu, Jiming Shi, Yanfei Jiang and Chang-Goo Kim for the usage of the “Athena++” MHD code. We also thank Haocheng Zhang for the helpful instruction of the “3DPol” polarization calculation code. We also thank helpful discussion and suggestions from Fan Guo, Haocheng Zhang, Xiangrong Fu and Shangfei Liu.

REFERENCES

- Akerlof, C., Balsano, R., Barthelmy, S., et al. 1999, *Nature*, 398, 400
 Blandford, R. D. 1976, *MNRAS*, 176, 465
 Daigne, F., & Mochkovitch, R. 1998, *MNRAS*, 296, 275
 Deng, W., Li, H., Zhang, B., & Li, S. 2015, *ApJ*, 805, 163
 Deng, W., Zhang, H., Zhang, B., & Li, H. 2016, *ApJ*, 821, L12
 Duffell, P. C., & MacFadyen, A. I. 2013, *ApJ*, 775, 87
 Fan, Y.-Z., Dai, Z.-G., Huang, Y.-F., & Lu, T. 2002, *ChJAA*, 2, 449
 Gao, H., Wang, X.-G., Mészáros, P., & Zhang, B. 2015, *ApJ*, 810, 160
 Gao, H., & Zhang, B. 2015, *ApJ*, 801, 103
 Gomboc, A., Kobayashi, S., Guidorzi, C., et al. 2008, *ApJ*, 687, 443-455
 Goodman, J. 1986, *ApJ*, 308, L47
 Kobayashi, S., Piran, T., & Sari, R. 1997, *ApJ*, 490, 92
 Kumar, P., & Panaitescu, A. 2003, *MNRAS*, 346, 905
 Kumar, P., & Zhang, B. 2015, *Phys. Rep.*, 561, 1
 Lan, M.-X., Wu, X.-F., & Dai, Z.-G. 2016, *ApJ*, 816, 73
 Lazzati, D. 2006, *New Journal of Physics*, 8, 131
 Liang, E.-W., Yi, S.-X., Zhang, J., et al. 2010, *ApJ*, 725, 2209
 Lovelace, R. V. E. 1976, *Nature*, 262, 649
 Lyutikov, M., & Blandford, R. 2003, *arXiv:astro-ph/0312347*
 McKinney, J. C., & Uzdensky, D. A. 2012, *MNRAS*, 419, 573
 Mészáros, P., & Rees, M. J. 1999, *MNRAS*, 306, L39
 Mészáros, P., & Rees, M. J. 2000, *ApJ*, 530, 292
 Mimica, P., Giannios, D., & Aloy, M. A. 2009, *A&A*, 494, 879
 Mizuno, Y., Zhang, B., Giacomazzo, B., et al. 2009, *ApJ*, 690, L47
 Mundell, C. G., Kopač, D., Arnold, D. M., et al. 2013, *Nature*, 504, 119
 Paczynski, B. 1986, *ApJ*, 308, L43
 Rees, M. J., & Meszaros, P. 1994, *ApJ*, 430, L93
 Rybicki, G. B., & Lightman, A. P. 1979, *New York, Wiley-Interscience*, 1979. 393 p.,
 Sari, R., & Piran, T. 1999, *ApJ*, 517, L109
 Steele, I. A., Mundell, C. G., Smith, R. J., Kobayashi, S., & Guidorzi, C. 2009, *Nature*, 462, 767
 Uzdensky, D. A., & MacFadyen, A. I. 2007, *ApJ*, 669, 546
 White, C. J., Stone, J. M., & Gammie, C. F. 2016, *ApJS*, 225, 22
 Zhang, B., & Kobayashi, S. 2005, *ApJ*, 628, 315
 Zhang, B., Kobayashi, S., & Mészáros, P. 2003, *ApJ*, 595, 950
 Zhang, B., & Yan, H. 2011, *ApJ*, 726, 90
 Zhang, H., Chen, X., Böttcher, M. 2014, *ApJ*, 789, 66
 Zhang, H., Deng, W., Li, H., & Böttcher, M. 2016, *ApJ*, 817, 63